

Aggregation Kernel Homogeneity for Fractal Aggregate Aerosols in the Slip Regime

G. M. Wang and C. M. Sorensen

Department of Physics and Program for Complex Fluid Flows, Kansas State University,
Manhattan, Kansas

A theoretical description of the aggregation kernel homogeneity for fractal aggregates in the slip regime is developed. Experimental values of the kernel homogeneity were determined with dynamic light scattering measurements on titania and silica aerosols at pressures of 1/10 to one atmosphere. These experiments yielded aggregates with a fractal dimension of ca. 1.75 and aggregate radii to cover a range of Knudsen numbers of 0.04–3.8. Measurement of the fractal aggregate mobility radius as a function of time during aggregation gave the homogeneity. Agreement of theory and experiment is in general successful.

INTRODUCTION

Aggregation is the fundamental process by which aerosols and colloids coarsen. Nature presents us with a rich variety of conditions under which aggregation can occur and the structures that result. When liquid particles aggregate, coalescence usually ensues to yield larger drops of the same spherical morphology. When solid particles aggregate, random structures form. The past two decades have seen that these random aggregates are nearly always describable as fractals with a universal fractal dimension D_f (Forrest and Witten 1979; Mandelbrot 1982; Viscek 1992). Fractal aggregates are well described by

$$N = k_o (R_g/a)^{D_f}, \quad [1]$$

where N is the number of monomer or primary particles in the aggregate, k_o is a constant of order unity, R_g is the radius of gyration of the aggregate, and a is the monomer radius. This variety in aggregate morphology is combined with a range of kinetic regimes in which the aggregation can occur. Colloids and many aerosols lie in the continuum regime in which the

ratio of the medium molecule mean free path to the particle radius, the so-called Knudsen number Kn , is very small. In this situation, aggregation occurs due to diffusive motion of the particles. Aerosols can have larger mean free paths, hence larger Knudsen numbers, but the particle motion can remain diffusive. The law of diffusion can be inverse size (at $Kn = 0$) to inverse size squared at large Kn . For very large Kn , ballistic motion dominates the paths between collisions and the aggregation kinetics changes again. The combination of variety in both morphology and kinetics makes aggregation rich in possibilities.

The fundamental description of irreversible coagulation and aggregation dynamics is the mean field Smoluchowski equation (Friedlander 1977)

$$\frac{\partial n(v, t)}{\partial t} = \frac{1}{2} \int_0^v K(v-u, u)n(v-u, t)n(u, t) du - n(v, t) \times \int_0^\infty K(v, u)n(u, t) du, \quad [2]$$

where $n(v, t)$ is the number density of aggregates with v monomers at time t , and $K(v, u)$ is the aggregation kernel which describes the rate at which aggregates with v and u monomers combine to form new aggregates with $v + u$ monomers. Unfortunately, exact solutions to Equation (2) exist only for a few simple $K(v, u)$. However, for many more complex physical situations, scaling solutions can be found because $K(v, u)$ can be a homogeneous function of its variables defined as

$$K(\gamma v, \gamma u) = \gamma^\lambda K(v, u), \quad [3]$$

where γ is a constant and λ is the degree of the kernel homogeneity. The homogeneity λ is very important because it is the key parameter in the scaling distribution of the aggregates and in the dynamics, through the dynamic exponent $z = (1 - \lambda)^{-1}$, which describes the asymptotic behavior, $N \sim t^z$ (see Equation (20), below).

Previous experimental work on aggregation kinetics has studied either the overall rate constant, the functionalities of the growth with time, or both. For liquid drop aerosols we mention here the work of Wagner and Kerker (1977), who established

Received 7 September 1999; accepted 5 February 2000.

This research was supported by National Science Foundation grant CTS 9709764.

Address correspondence to Christopher M. Sorensen, Department of Physics, 116 Cardwell Hall, Kansas State University, Manhattan, KS 66506-2601.

the validity of the aggregation rate in the slip regime for liquid drops with Knudsen numbers as large as 12. The temporal functionalities were not studied in the scaling regime of the size distribution, however, so λ as not determined. Previously in our laboratory (Olivier et al. 1992), we solely used nonperturbative light scattering measurements to study a liquid drop aerosol with $\text{Kn} \leq 0.26$ and found the rate constant in agreement with theory and, from the temporal functionalities, $\lambda = 0.07 \pm 0.06$.

Fractal aggregation kinetics studies date back to work by Weitz et al. (1984), who studied gold colloids and found a temporal dynamics of $R \sim t^{1/D_f}$, where R is a radius of the aggregate for Diffusion Limited Cluster Aggregation (DLCA) aggregates with $D_f \approx 1.75$. Since dynamic light scattering was used and this technique measures the diffusion coefficient, R must be the mobility radius. The implication of this result is that $\lambda = 0$, expected in a colloid where $\text{Kn} \ll 1$ and diffusion is the rate limiting step. Subsequent work (Weitz et al. 1985; Lin et al. 1990) showed that a reaction limited regime exists as well where $R \sim e^t$ to imply $\lambda \rightarrow 1$. Between these regimes exists either a crossover (Lin et al. 1990) or a continuous evolution of λ from 0 to 1 (Olivier and Sorensen 1990). None of the work on colloidal fractal aggregation measured the rate coefficients of the aggregation. Work on fractal aggregation beyond the continuum regime, i.e., $\text{Kn} > 0$, is limited. Those studies that do exist involve light scattering studies of soot particles in flames, but only a recent study from this laboratory (Oh and Sorensen 1997) combined current understanding of fractal aggregate light scattering and an analysis accounting for the fractal morphology in the aggregation kernel. In our work we found a slightly enhanced aggregation rate for $D_f \approx 1.89$ fractal aggregates in the crossover regime between ballistic and diffusional aggregate motion.

With previous work as a background, there is a need to study the complex temporal dependencies for fractal aggregation when $\text{Kn} > 0$. In this paper we present a new theoretical description of the kernel homogeneity in the slip regime for DLCA aggregates with $D_f \approx 1.75$ and present light scattering data obtained from aggregating aerosols to substantiate this description. Our description is consistent with the continuum and free molecular regimes in the limits of $\text{Kn} \ll 1$ and $\text{Kn} \gg 1$, respectively. In describing the aggregation kernel we will show that complexities arises from two sources: 1) the crossover of the diffusion coefficient from inverse radius to inverse radius squared dependencies, which occurs regardless of the fractal nature, and 2) the behavior of the mobility radius of a fractal aggregate, which we have recently found (Wang and Sorensen 1999) is related to both the free molecular to continuum crossover and the small particle limit.

THEORY

The Aggregation Kernel

The aggregation kernel describes the rate at which two aggregates come together and combine to form a larger aggregate. This rate depends on the relative motion of the aggregates and

their size. In this work we consider only diffusive motion, not ballistic motion which can occur in very rarified situations. With diffusive motion, the aggregation kernel is

$$K(u, v) = 4\pi[D(u) + D(v)][R(u) + R(v)]. \quad [4]$$

In Equation (4), $D(u)$ is the diffusion coefficient and $R(u)$ is the radius, to be defined below, of an aggregate with u monomers.

For spherical particles the radius in Equation (4) is simply the geometric radius. The diffusion coefficient depends on the kinetic regime which is parameterized by the Knudsen number, Kn (Friedlander 1977). For $\text{Kn} \ll 1$ the continuum regime is obtained and the Stokes–Einstein equation holds:

$$D_{SE} = \frac{kT}{6\pi\eta R}. \quad [5]$$

In Equation (5), k is Boltzmann's constant, T is the absolute temperature, and η is the shear viscosity of the medium. When $\text{Kn} \gg 1$, the free molecular regime is obtained and the Epstein equation holds:

$$D_{Ep} = \frac{3}{8\rho R^2} \left(\frac{mkT}{2\pi} \right)^{1/2} \left(1 + \frac{\pi}{8}\beta \right)^{-1}. \quad [6]$$

In Equation (6), ρ is the gas medium mass density, m is the gas molecule mass, and $0 \leq \beta \leq 1$ is the accommodation coefficient.

In the “slip” regime where $\text{Kn} \sim 1$, the Cunningham correction factor can be applied to the Stokes–Einstein form in Equation (5) to allow a continuous description of the diffusion coefficient between the two limits represented by Equations (5) and (6). Recently, we have proposed a simpler interpolation scheme that, when compared to the original data, works nearly as well (Sorensen and Wang 1999). We write

$$D = D_{SE}[1 + A \text{Kn}] \quad [7]$$

or equivalently

$$D = \frac{kT}{6\pi\eta(mfp)}[\text{Kn} + A \text{Kn}^2]. \quad [8]$$

In Equations (7) and (8), $A = 2.25/(1 + \beta\pi/8)$ and mfp in Equation (8) is the mean free path of the medium molecules. The simplicity of these equations makes analysis of the aggregation kernel in the slip regime easier than with the Cunningham correction factor. They also allow us to make an important approximation regarding the homogeneity in the slip regime, which we describe below.

For fractal aggregates application of Equation (4) requires an understanding of both the diffusive mobility (first term) and the geometric size (second term) of the aggregate (Mulholland et al. 1988; Matsoukas and Friedlander 1991; Rogak and Flagan 1992). For the geometric size we shall use a proportionality to

the radius of gyration which, unlike a perimeter radius, can be precisely defined for an aggregate. We write

$$R = cR_g, \quad [9]$$

where c is a constant of order unity. For fractal dimensions $D_f > 2$, aggregates are projectionally opaque so no cluster could possibly pass through another cluster and Equation (9) should hold. For D_f not too much smaller than 2, e.g., $D_f \approx 1.75$, however, a planar projection of the aggregate would have holes indicating the possibility of one cluster passing through another, and then Equation (9) would fail. However, the clusters rotate as well as diffuse and rotational averaging would eliminate these holes. Moreover, diffusion of a cluster through a projectional hole of another seems very unlikely; a projection requires a straight path. These arguments indicate that a given aggregate sees another aggregate as a blur of size R_g . Finally, following others, we remark that since $R_g \sim N^{1/D_f}$ when $D_f < 2$, the aggregate cross section is greater than the sum of the individual monomer cross sections, but unlike others, we claim that with rotational averaging this is not unphysical. Thus we conclude Equation (9) holds for DLCA aggregates, and perhaps for all D_f .

The diffusion of a fractal aggregate can be described with Equations (7) or (8) with R replaced by R_m , the mobility radius of the aggregate. This replacement defines R_m as the radius of a spherical particle with the same diffusion coefficient as the aggregate. It is easy to show (Sorensen and Wang 1999) that this forces us to define the Knudsen number in terms of the mobility radius as

$$\text{Kn} = mfp/R_m. \quad [10]$$

In previous work we used the radius of gyration in Equation (10), but we now believe this is not as facile a definition as that using R_m . We propose that Equation (10) applies to *all* particles, viz. spheres, aggregates, etc.

To proceed, the characteristics of R_m for a fractal aggregate have to be determined. In recent work we have addressed this issue experimentally (Wang and Sorensen 1999). It is convenient to describe R_m relative to the well-defined radius of gyration as the ratio R_m/R_g . We have found that R_m/R_g increases with D_f . Here we will consider only DLCA aggregates, which are very common, with $D_f \approx 1.75$. The dependency of R_m/R_g on the kinetic regime, parameterized by Kn, is detailed, and we describe it with the aid of Figure 1. This figure is similar to Figure 8 of Wang and Sorensen (1999), where we first discussed these results, only now we use the Knudsen number defined with R_m rather than R_g . To begin our description consider an "aggregate" containing only one spherical particle, i.e., $N = 1$. Then the mobility radius is the sphere's geometric radius R , and the radius of gyration (the mean square radius) can be shown to be $R_g = \sqrt{3/5}R$. Thus $R_m/R_g = \sqrt{5/3} = 1.29$ in the aggregate's single sphere ($N = 1$) limit regardless of Kn. A dotted line in Figure 1 marks this limit. When $\text{Kn} \gg 1$, it has

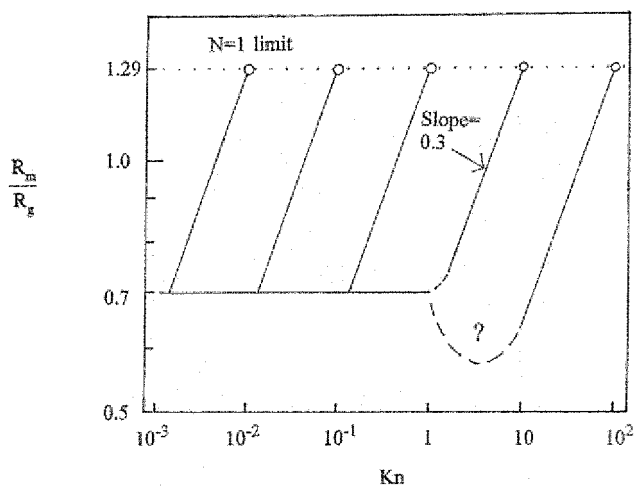


Figure 1. Schematic diagram for the ratio R_m/R_g for a fractal aggregate with $D_f = 1.75$ as a function of the Knudsen number $\text{Kn} = mfp/R_m$. All functionalities on Kn start at the single sphere ($N = 1$) limit and then proceed to smaller Kn with larger N , where N is the number of monomers per aggregate.

been established empirically that (Meakin et al. 1989; Cai and Sorensen 1994)

$$R_m = aN^x \quad [11]$$

with $x = 0.44 \pm 0.03$. We discussed how for small N this agrees very well with a calculation by Chan and Dahneke (1981) for straight chains. Since $R_g = a(N/k_o)^{1/D_f}$ via Equation (1), then $R_m/R_g = k_o^{1/D_f} N^{x-1/D_f}$. This result forces $k_o = 1.56$ when $D_f = 1.75$ via the $N = 1$ limit (recall, $R_m/R_g = 1.29$), a value consistent with previous work from this laboratory. For Figure 1 we express the functionality on N in terms of the Knudsen number $\text{Kn} = mfp/R_m \sim N^{-x}$. Then, for $D_f = 1.75$,

$$R_m/R_g \sim \text{Kn}^{(1-xD_f)/xD_f} \quad [12a]$$

$$= \text{Kn}^{0.30} \text{ for } \text{Kn} \gg 1. \quad [12b]$$

Following Wang and Sorensen (1999), the description of R_m/R_g for a fractal aggregate as a function of N starts with the $N = 1$, monomer limit of $R_m/R_g = 1.29$. The Knudsen number of the monomer depends on its size and the mean free path of the medium. In the other limit of large aggregates Kn will be in the continuum regime where we have found that $R_m/R_g = 0.70 \pm 0.05$, a constant. Thus, as N increases from one, R_m/R_g must evolve from 1.29 to 0.70, but the manner in which this occurs can be complex. If the Knudsen number for the monomer, which we will call the monomer Knudsen number, is large, R_m/R_g will drop away from 1.29 with decreasing Kn in accord with Equation (12). Note that when the monomer Kn is $> (1.29/0.7)^{1/0.3} \approx 8$, the ratio R_m/R_g can evolve to values < 0.7 before the continuum regime is entered. Then further

increase in N , hence decrease in Kn , would necessitate the ratio to increase with decreasing Kn in order to join with the continuum value of 0.7. For clusters with monomer $\text{Kn} \leq 1$, the fall from 1.29 to 0.7 with decreasing Kn is monotonic, but the functionality is unknown. Here we assume that the functionality is the same as in the $\text{Kn} > 1$ regime, viz., Equation (12), and this is consistent with data near $\text{Kn} \lesssim 1$ (Wang and Sorensen 1999). Figure 1 sketches the behavior of R_m/R_g versus Kn for a variety of initial monomer Knudsen numbers.

The aggregation kernel for a fractal aggregate is a combination of the considerations above applied to Equation (4). The interplay of the diffusion coefficient of Equation (8) and the mobility radius described in Figure 1 is somewhat complex, but straightforward. Scaling arguments could be made to determine the dynamic exponent $z = 1/(1-\lambda)$ based on the functionalities of D , R_m , and R_g on size N if the kernel was homogeneous; but it is not. The slip regime, $\text{Kn} \sim 1$, finds the diffusion coefficient crossing over from an inverse R to an inverse R -squared dependency, which results in an inhomogeneous function. This is obvious with an inspection of Equation (8) and results regardless of the mathematical description of the crossover. Thus a simple description of scaling and the dynamics in the $\text{Kn} \sim 1$ regime seems lost.

Despite these problems, we will persevere with an approximation. A log-log plot of D versus Kn , shown in Figure 2a, crosses over from a slope of one to two. D is a homogeneous function of Kn in the large and small limits with homogeneity equal to the slope on this plot. Our approximation is that D is a homogeneous function of Kn for any Kn and the degree of homogeneity is the slope of this plot. We call the slope s , hence $D \sim \text{Kn}^s$ and the slope is plotted in Figure 2b.

The degree of homogeneity of the kernel to be used to determine the scaling dynamics of the aggregation is its power-law functionality on N . To determine this, first write Equation (4) combined with Equation (9) as

$$K \sim DR_g. \quad [13]$$

By (1), we have $R_g \sim N^{1/D_f} = N^{0.57}$. The functionality of D on N is a combination of the approximation $D \sim \text{Kn}^s$ and the functionality of R_m on N , which is determined by the behavior of the ratio R_m/R_g in Figure 1. This plot is reproduced in Figure 2c. There are perhaps many ways to plot these parameters, but we have found that using Kn as an independent variable, rather than N , keeps track of the kinetic regime for both D and R_m . Moreover, use of the ratio R_m/R_g unifies the mobility relative to the value of 0.7 when $\text{Kn} < 1$.

Values for the kernel homogeneity can now be calculated using Figures 2a, b, and c and the equation

$$\lambda = -sx + 1/D_f. \quad [14]$$

Recall that $x = 1/D_f \approx 0.57$ for $\text{Kn} < 1$ and 0.44 for $\text{Kn} > 1$. For example, consider when the monomer $\text{Kn} = 100$. Then for

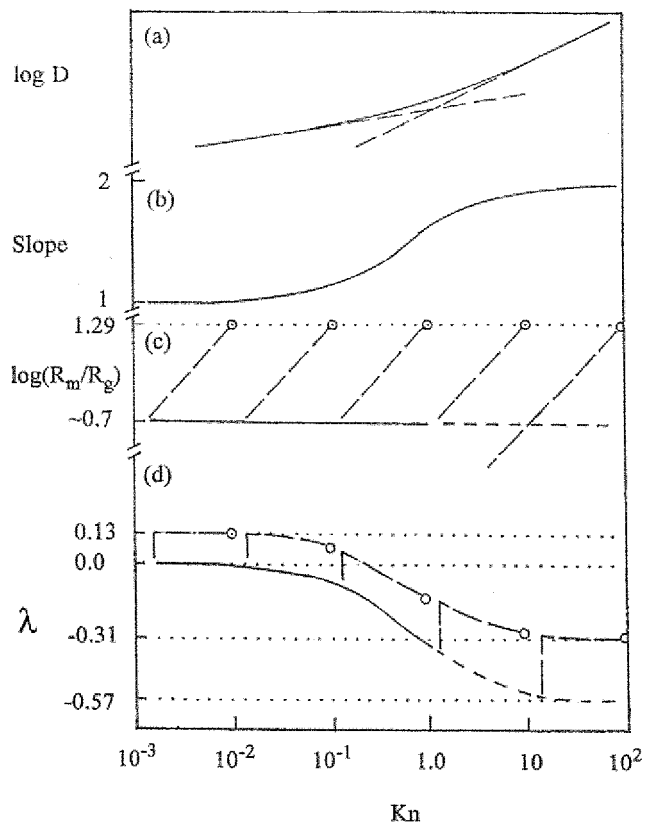


Figure 2. Graphical procedures to determine the effective aggregation kernel homogeneity. a. Diffusion coefficient D as a function of Knudsen number $\text{Kn} = mfp/R_m$ as described by either Equation (7) or (8). b. Slope of D versus Kn . c. R_m/R_g versus Kn as described in Figure 1. d. The kernel homogeneity λ versus Kn . In (c) and (d) the short-dashed, long-dashed, and solid lines correspond to each other. The short-dashed behavior probably does not occur but is a useful reference at large Kn . The sharp cross overs in (c) from long-dashed to straight line behavior leads to discontinuous jumps in λ in part (d). Physically, these transitions are no doubt smoother but their functionality is unknown.

small N , Figure 2b yields $s = 2$, and Figure 2c shows that R_m/R_g is still slopping away from the monomer value, thus $R_m/R_g \sim \text{Kn}^{0.30}$ to imply $R_m \sim N^{0.44}$ (Equation (11)). Equation (13) implies $K \sim (N^{0.44})^{-s} N^{0.57}$, thus Equation (14) is $\lambda = -0.44s + 0.57 = -0.31$. As N increases, Kn for the aggregate decreases and the slope s decreases from 2. This causes λ to grow less negative as drawn in Figure 2d with the long-dashed line. Difficult to describe is the “turn around” near $\text{Kn} \gtrsim 1$ where R_m/R_g must increase with decreasing Kn . This would cause $\lambda < -0.31$, but we are unable to quantify this with our present knowledge. After this turn around, when the aggregate is large enough so that $\text{Kn} \sim 1$, then $R_m/R_g \approx 0.7$, a constant, to yield $R_m \sim N^{1/D_f}$. Then the functionality of λ with Kn follows the solid line, which near $\text{Kn} \approx 1$ (Equation (14))

yields $\lambda = -0.34$ since $s \approx 1.6$. A second example is for a monomer $\text{Kn} = 0.1$. Then from Figure 2b for small N , $s \leq 1.12$, and we assume the same power law for R_m/R_g as used when $\text{Kn} > 1$. Then $K \sim (N^{0.44})^{-1.12} N^{0.57}$ and Equation (14) yields $\lambda = 0.08$. As Kn for the aggregate declines (due to increasing N) the slope s falls to one, hence λ follows the long-dashed line to approach 0.13. However, once the fall from the monomer value of $R_m/R_g = 1.29$ reaches the limiting behavior of 0.7, the functionality of λ must cross over to the solid line in Figure 2d. For all situations when $\text{Kn} \ll 1$, $R_m \sim R_g$, thus $K \sim (N^{0.57})^{-s} N^{0.57}$, which for $s = 1$ yields $\lambda = 0$ by Equation (14). With such reasoning we constructed Figure 2d, a graph of the kernel homogeneity versus aggregate Knudsen number for fractals with $D_f = 1.75$.

The Scaling Solution and the Dynamics

At sufficiently long times, the homogeneity condition (3) allows so-called scaling (van Dongen and Ernst 1985) or self-preserving (Friedlander and Wang 1966; Lai et al. 1972; Lushnikov 1973; Friedlander 1977) solutions to the Smoluchowski Equation (2) of the form

$$n(v, t) = M_1 s_p^{-2} \phi(\hat{v}). \quad [15]$$

In Equation (15) \hat{v} is the normalized or reduced size

$$\hat{v} = \frac{v}{s_p} \quad [16]$$

and s_p is one of a class of mean sizes indexed by p and defined by

$$s_p(t) = \frac{M_p}{M_{p-1}}, \quad [17]$$

where the unnormalized i th moment of the size distribution is given by

$$M_i(t) = \int_0^\infty v^i n(v, t) dv. \quad [18]$$

Note that the size s_p is a mean number of monomers per aggregate, $\langle N \rangle$. Also in Equation (15) is the reduced size distribution function $\phi(\hat{v})$ given by

$$\phi(\hat{v}) = A \hat{v}^\lambda e^{-\alpha \hat{v}} \quad [19]$$

for large \hat{v} . The shape of $\phi(\hat{v})$ is not a function of time, hence the distribution is "self-preserving." The time dependence resides solely in the mean size $s_p(t)$. The large x regime is all we need to be concerned with in our study because light is scattered predominantly from the large size part of the cluster distribution. Moreover, the nature of the aggregation kernel in all three kinetic regimes is such that "bell shaped" distributions result, characterized by exponentially decreasing cluster populations with decreasing size when $\hat{v} < 1$ (van Dongen and Ernst 1985).

The parameters A and α in Equation (19) are determined by normalization of the size distribution and the definition of the mean size s_p through p . Some detail is given in Oh and Sorensen (1997).

A colligative measurement such as light scattering measures a moment of the distribution, M_i in Equation (18), not the distribution itself, $n(v)$. Thus we must understand the time evolution of the moments. For those aggregates whose size distribution has reached a scaling or self-preserving form, the time evolution of the moments of the size distribution is given by (Olivier et al. 1992; Oh and Sorensen 1997)

$$M_i(t) = M_i(t_0)[1 + (t - t_0)/t_c]^{(i-1)z}. \quad [20]$$

In Equation (20), t_0 is any chosen time after the size distribution has achieved a scaling form, and t_c is the characteristic aggregation time and is related to the aggregation kernel. Also in Equation (20), the kinetic exponent z equals

$$z = \frac{1}{1 - \lambda}. \quad [21]$$

By Equation (17) the mean size of an aggregate is a ratio of moments of consecutive order. Thus in general it follows from Equations (17) and (20) that at long time

$$s_p \propto t^z. \quad [22]$$

From (1) it then follows that $R_g \sim t^{z/D_f}$.

In this work we measure the mobility radius R_m with dynamic light scattering. As discussed above and displayed in Figure 1, the dependency of R_m on the mean size is not as simple as for R_g . This dependency is given in Equation (11) and x can be either ≈ 0.44 when $\text{Kn} \gg 1$, or since $R_m \approx 0.7R_g$ when $\text{Kn} < 1$, $x = 1/D_f \approx 0.57$ in the continuum regime. Given this we can write

$$R_m(t) = R_m(t_0)[(1 + (t - t_0)/t_c)]^{xz}. \quad [23]$$

EXPERIMENTAL METHODS

Both TiO_2 and SiO_2 aerosols were used in this study. The aerosols were generated by thermal decomposition of either titanium tetraisopropoxide (TTIP) or tetraethyl orthosilicate (TEOS), similar to the method reported by Okuyama et al. (1986). Vapors were generated by heating TTIP or TEOS to temperatures around 80°C and 30°C , respectively, and then these were carried into a half meter long tube furnace by dry N_2 gas with a flow rate of 0.5 l/min. The furnace was set to a temperature of $\sim 400^\circ\text{C}$ or $\sim 900^\circ\text{C}$, respectively. The vapors decomposed inside the furnace to form particles ($\sim 35 \pm 10$ nm in diameter, see transmission electron microscope image in Figure 3) and carried out of the furnace as an aerosol.

A stainless steel cylindrical chamber ($ID = 20$ cm, height = 35 cm) was used to contain the fresh aerosol. At the middle

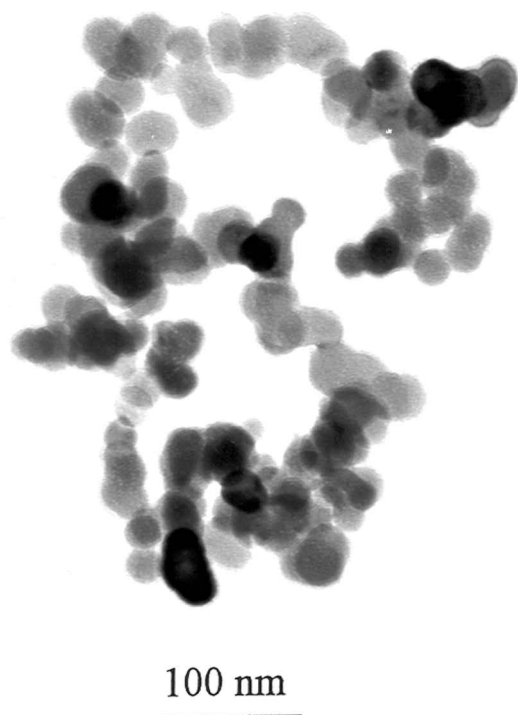


Figure 3. TEM image of a fresh TiO_2 aerosol aggregate.

height of the chamber, a curved glass window allowed for light scattering measurements at scattering angles from $\theta = 0$ to 120° .

For the aerosol inside the chamber, the mean free path of the medium gas (a mixture of air and dry N_2) was about 65 nm at ambient temperature and one atmosphere of pressure. On the other hand, R_m for the aggregates ranged from 145 nm to 1600 nm. Thus Kn under these circumstances was between 0.04 and 0.45. In order to expand the Kn range, the chamber pressure was reduced from 1 atmosphere pressure to 1/2, 1/3, 1/5, and 1/10 atmospheric pressure. This increased the mean free path to as much as 650 nm. As a result, Kn was extended to values as large as 3.8.

Light scattering was performed by employing a vertically polarized Ar ion laser with wavelength $\lambda_0 = 488$ nm. Static structure factor measurements were made at scattering angles from 3 to 120° (Sorensen 1997). Dynamic light scattering used an ALV5000 digital autocorrelator with the photomultiplier tube (detector) normally placed at scattering angles between 20 and 90° .

RESULTS AND DISCUSSION

Static Light Scattering

To verify that the generated aerosol contained well characterized DLCA aggregates, static light scattering was carried out on the aerosols. A typical measurement for an aerosol at atmospheric pressure is presented in Figure 4. This graph is a log-log plot of the structure factor, $S(q) = I(q)/I(0)$, where

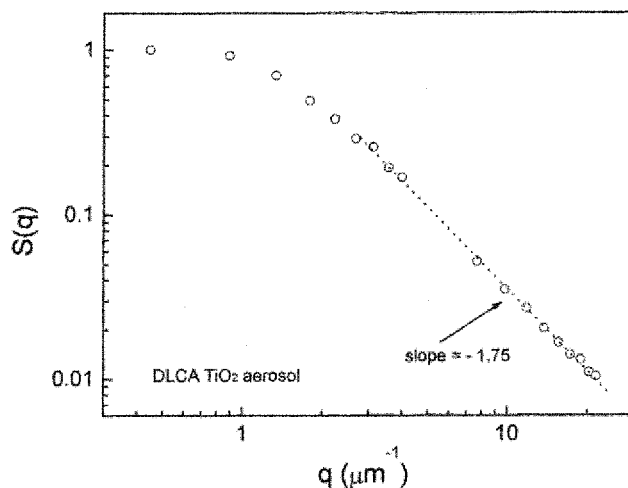


Figure 4. Structure factor of TiO_2 aerosol aggregates measured by static light scattering, which shows a fractal dimension of 1.75 ± 0.1 .

I is the scattered intensity, of the aerosol versus the scattering wave vector q . The scattering wave vector is

$$q = 4\pi\lambda_0^{-1} \sin\left(\frac{\theta}{2}\right), \quad [24]$$

where λ_0 is the wavelength of light. This particular run shows the investigated aerosol had an average $R_g \sim 790$ nm. A linear fit to the power law regime for $qR_g > 4$ yielded a slope of -1.75 ± 0.1 , which equals $-D_f$. This D_f value agrees well with the commonly accepted fractal dimension for DLCA aggregates.

Dynamic Light Scattering

Dynamic light scattering measures the scattered light intensity autocorrelation function, $C(t) = \langle I(t)I(0) \rangle$, as a function of lag time t (Berne and Pecora 1976). In general, this autocorrelation decays exponentially with lag time due to diffusive motion of the aggregate. Hence

$$C(t) = B_0 + B_1 e^{-t/\tau_c}, \quad [25]$$

where B_0 is background signal, B_1 is a constant, and τ_c is the correlation time. Fitting to the autocorrelation curve will yield τ_c , which is linked to the diffusion coefficient D of the aggregate (Berne and Pecora 1976)

$$\tau_c = (2Dq^2)^{-1}. \quad [26]$$

Figure 5 shows selected DLS measurements carried out at 1/10 atmospheric pressures for the TiO_2 aerosol. There are two apparent decays in the autocorrelation curve: one in a small time region ($t < 0.5$ ms) and another in a larger time region ($t > 20$ ms). Analysis shows that the first decay is exponential and related to aggregate diffusive motion, hence it contains τ_c .

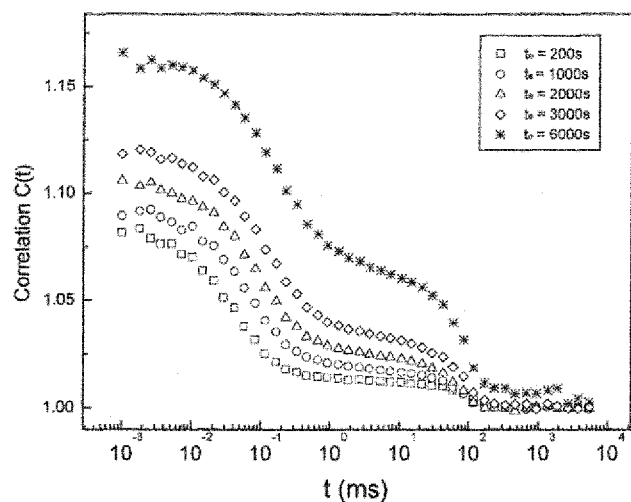


Figure 5. Scattered light intensity autocorrelation function of a TiO_2 aerosol at 1/10 atmospheric pressure as a function of time. t_{exp} is the experimental run time, i.e., the time after chamber filling when the measurement of $C(t)$ was made. Each measurement took ca. 20 s.

The second decay has a Gaussian shape and is associated with density fluctuations (Schaefer and Berne 1972). As the experiment progressed (larger t_{exp}), the first decay shifted to larger time, indicating an increase in R_m due to aggregation. Concurrently, the second decay also became more apparent with time. This is associated with the aggregation process as well, since as the clusters became bigger during aggregation, the number density decreased. As a result, the density fluctuation increased.

To determine the characteristic correlation time τ_c , all DLS runs were fit to a sum of an exponential and a Gaussian term for the reasons explained above. A fit to the data in Figure 5 by this two-term fit is shown in Figure 6 (dashline). As can be seen, a reasonable fit was achieved in the first and second decay regimes. However, a misfit is clearly visible in the intermediate regime $1 < t < 20$ ms. In order to improve the accuracy of the fitting, a third exponential term was added ad hoc. Hence the scattered light autocorrelation $C(t)$ was fit finally by three terms:

$$C(t) = B_0 + B_1 e^{-t/\tau_c} + B_2 e^{-t^2/\tau_2^2} + B_3 e^{-t/\tau_3}, \quad [27]$$

where B_3 and τ_3 are two additional fit variables for the ad hoc term. As discussed in our previous paper (Wang and Sorensen 1999), the ad hoc term may be related with some extra large clusters in the aerosol that break off from the furnace wall and are not associated with the aerosol aggregation. As shown in Figure 6 (solid line), this three-term fit matches the experimental data well. Once the correlation time τ_c was measured by DLS, Equation (6) (or (7)) with Equation (10) was used to determine R_m .

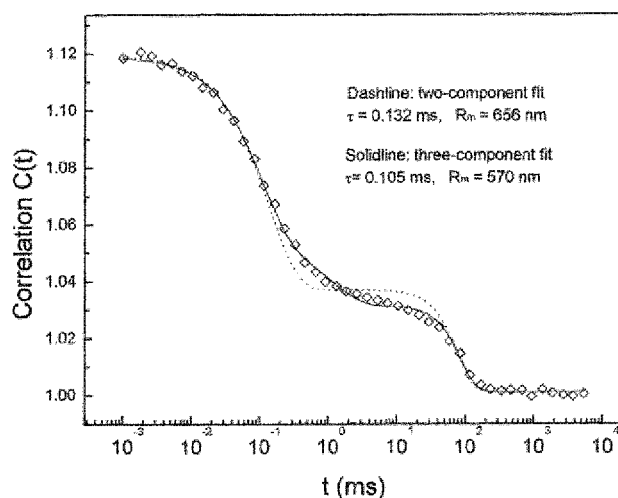


Figure 6. Computer fits to the dynamic light scattering data of Figure 5.

The Kernel Homogeneity

The R_m data for the three TiO_2 aerosols are plotted in Figure 7 in accord with Equation (23). Filling the aerosol chamber takes approximately 2 min so we will assume that the aerosols have achieved scaling distributions by the time we begin taking the DLS measurements; thus we set $t_0 = 0$. This assumption is not critical because even if the scaling distribution is not precisely achieved (and, indeed, only a quasi-self-preserving distribution is achieved in the slip regime, see Wang and Friedlander (1967), Equation (23) holds to a good approximation, and because the large time data dominate the fit. Normalizing by $R_m(0)$

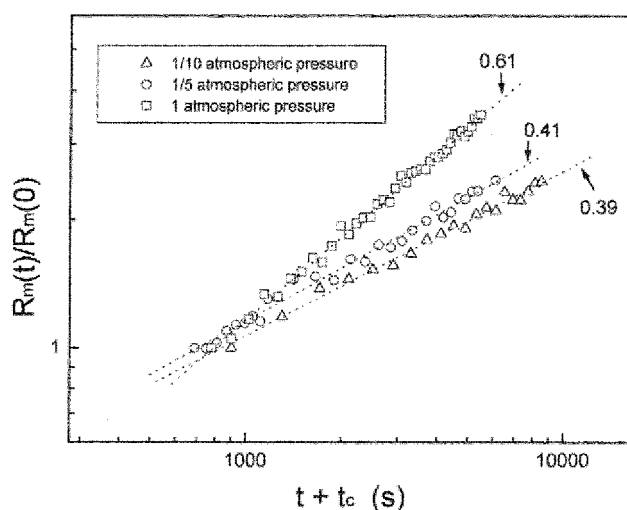


Figure 7. Normalized mobility radius for the TiO_2 aerosol as a function of time t plus the characteristic time t_c adjusted to make these log-log plots most linear. Dashed lines are fits with slopes z_x .

Table 1
Experimental Parameters for the Aerosol Systems

Aerosol material	Pressure (atm)	$R_m(0)$ (nm)	$R_m(f)$ (nm)	Kn(0)	Kn(f)	$N(0)$	$N(f)$	$R_m(0)/a$	zx	λ
TiO ₂	1/10	320	800	2	0.8	370	1850	18	0.39 ± 0.03	-0.46 ± 0.1
TiO ₂	1/5	180	450	1.8	0.7	140	680	10	0.41 ± 0.03	-0.38 ± 0.1
TiO ₂	1	145	510	0.45	0.13	90	840	8	0.61 ± 0.05	0.05 ± 0.08
SiO ₂	1/10	170	400	3.8	1.6	120	550	9	0.40 ± 0.03	-0.43 ± 0.1
SiO ₂	1/10	210	420	3.1	1.5	180	600	12	0.41 ± 0.03	-0.40 ± 0.1
SiO ₂	1/3	240	670	0.3	0.8	220	1400	13	0.42 ± 0.03	-0.34 ± 0.10
SiO ₂	1/2	180	400	0.32	0.7	140	550	10	0.47 ± 0.05	-0.22 ± 0.10
SiO ₂	1/2	240	800	0.16	0.54	220	1900	13	0.54 ± 0.03	-0.05 ± 0.07
SiO ₂	1/5	170	380	1.9	0.85	120	500	9	0.44 ± 0.03	-0.28 ± 0.1
SiO ₂	1/5	150	350	2.2	0.93	100	440	8	0.42 ± 0.03	-0.36 ± 0.1
SiO ₂	1	270	1600	0.24	0.04	280	6200	15	1.63 ± 0.03	0.08 ± 0.05
SiO ₂	1	250	1300	0.26	0.05	240	4300	14	0.54 ± 0.03	-0.05 ± 0.06
SiO ₂	1	280	1000	0.23	0.06	300	2700	16	1.58 ± 0.03	0.01 ± 0.05

Equation (23) becomes

$$R_m(t)/R_m(0) = [(t_c + t)/t_c]^{zx}. \quad [28]$$

This equation shows that a log-log plot of $R_m(t)/R_m(0)$ versus $t + t_c$ will be linear with the proper choice of t_c . Thus our fitting procedure is to vary t_c until this plot is linear; this yields the best fit t_c and the slope of the plot yields the exponent zx . The best linear fits to the graphs were obtained with $t_c = 950$ s, 650 s and 650 s for the 1/10, 1/5, and 1 atm aerosols, respectively. No quantitative meaning can be inferred from these numbers without a measure of the aerosol number density as well. However, the slopes of these linearized plots is zx of Equation (28), which we find to be 0.39 ± 0.03 , 0.41 ± 0.03 , and 0.61 ± 0.05 , respectively. These along with the values for the other runs are listed in Table 1.

Also listed in Table 1 are the ranges of the measured mobility radius, the Knudsen number, and the number of monomers per aggregate, N . This latter parameter was calculated using Equation (1), with $k_0 = 1.3$ (Cai et al. 1994; Sorensen and Roberts 1997; Oh and Sorensen 1997b), the measured (from TEM) monomer radius, $a = 18$ nm for both aerosols, $R_g = R_m/0.7$ (a fact confirmed below), and $D_f = 1.75$. The large N values show the aggregates are mature and justify our use of scaling relations. The Knudsen numbers show that the experiments are definitely in the slip regime.

To obtain the dynamic exponent z , hence the kernel homogeneity λ via Equation (21), from the data, the value of x of Equation (11) must be known.

The value of x is either 0.44 or $1/D_f \approx 0.57$ depending on whether R_m/R_g is evolving away from its monomer value, represented by the lines with slope 0.3 in Figure 1, or whether R_m/R_g is a constant, the zero slope line at $R_m/R_g = 0.7$ in Figure 1. The sloped regions in Figure 1 occur for values of R_m between $R_m = a$, the monomer limit, and $R_m = a(1.29/0.7)^{1/0.3} \approx 8a$. Listed in Table 1 is $R_m(0)/a$, and we see that initially for all aerosols

$R_m(0) > 8a$, thus all aerosols are in the constant $R_m/R_g = 0.7$ regime, hence $x \approx 0.57$. The dynamic exponent z and concomitant kernel homogeneity λ can now be calculated and the values of λ are given in Table 1 as well.

Figure 8 compares the measured homogeneities to theory as prescribed by Figure 2 and expressed in Equation (14). Theory requires the value of x and, as described above, since $R_m(0)/a > 8$

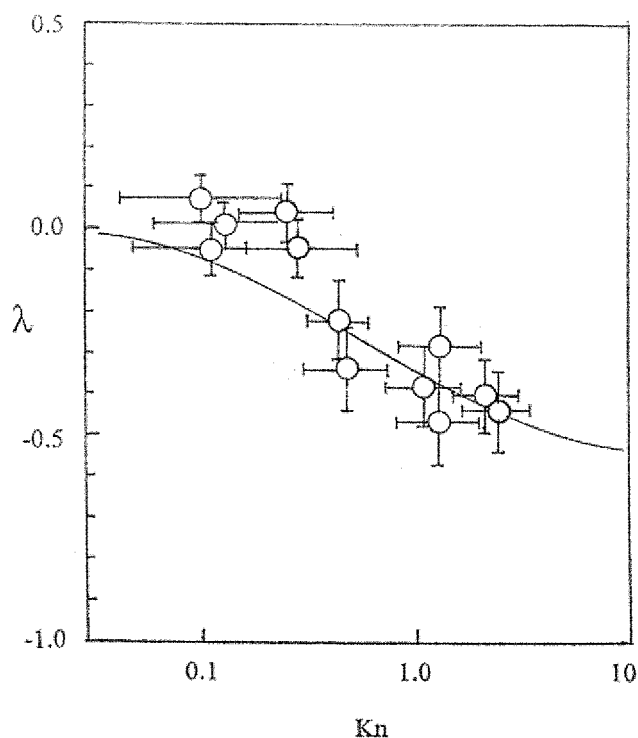


Figure 8. Comparison of the theoretically predicted kernel homogeneity λ from Figure 2d to experiment as tabulated in Table 1. The theoretical prediction is the solid line of Figure 2d, which corresponds to $R_m/R_g \approx 0.7$, a constant.

for all the aerosols, we expect $R_m/R_g = 0.7$, a constant and therefore $x = 0.57$. Then theory predicts for λ the solid line in Figure 2d, and this is reproduced in Figure 8. The data with their error bars in λ and their ranges in Kn show the decreasing trend in λ with increasing Kn as predicted. The agreement is quantitative, within error. Since R_m/R_g is constant, the functionality of λ in Figure 8 is due to the transition of the diffusion coefficient from R_m^{-1} to R_m^{-2} functionality through the slip regime. Our primary assumption was that this would yield a kernel that could still be described as homogeneous with an effective homogeneity dependent on the slope of $\log D$ versus R_m (Figure 2b). The fact that the data show this predicted functionality for the effective homogeneity thus lends veracity to the assumption.

Some deviation between theory and experiment, on the edge of the measurement error, is seen for $K_n \sim 0.1$, with the experimental λ being about 0.1 too large. This result is similar to a result from our recent work (Sorensen and Wang 1999), in which we showed how the power-law regime of the structure factor could be used to measure the width of the aggregate size distribution. For the scaling distribution the width parameter is the homogeneity λ as seen in Equations (19) and (15). We measured the structure factor for five titania aerosols at atmospheric pressure, conditions identical to those used here. We then applied our analysis of the power law regime to determine the width parameter λ . The average of the five aerosols was $\lambda = 0.24 \pm 0.23$. This is consistent with the dynamically determined value here of $\lambda = 0.02 \pm 0.06$ (average of the four one atmosphere aerosols). The theoretical curve in Figure 8, however, predicts $\lambda = -0.08$ for $\text{Kn} = 0.1$. Furthermore, our past work on liquid drop aerosols (Olivier et al. 1992) found from dynamical measurements $\lambda = 0.07 \pm 0.06$ when $\text{Kn} \sim 0.2$. As for the fractal aggregates of this work, the liquid drops of our previous work should have a diffusion coefficient crossing over from Stokes–Einstein ($D \sim R^{-1}$) to Epstein ($D \sim R^{-2}$). Hence λ should follow a curve similar to that drawn in Figure 8 only with a large Kn limit of $\lambda = -1/3$. Then for $\text{Kn} = 0.2$ we can predict $\lambda = -0.15$ for liquid drops, and once again the experimental value of λ is somewhat too large.¹ Thus there are three separate indications, all on the edge of the experimental error, that the kernel homogeneity near $\text{Kn} \sim 0.1$ is larger than predicted here. We do not know the source of this possible discrepancy.

CONCLUSIONS

The primary results of this paper are the predictions for the aggregation kernel homogeneity λ over the entire Knudsen number range as depicted in Figure 2 and expressed by Equation (14) and the experimental verification in the difficult slip regime as shown in Figure 8. Uncertainties remain in the functionality $R_m \sim N^x$ (Equation (11)) in the $\text{Kn} < 1$ range when the aggregate is still falling away from the single particle limit (i.e., when

R_m/R_g is not yet constant), the nature of the crossover from this dependency to the constant $R_m/R_g \simeq 0.7$, and the turn around in R_m/R_g at large Kn. The approximation that the kernel is homogeneous in the slip regime with a homogeneity dependent upon the approximate power-law dependency of the diffusion coefficient on aggregate mobility radius (the slope in Figures 2b and c) appears to be valid. Computer simulation testing of these results would be valuable.

REFERENCES

- Berne, B., and Pecora, R. (1976). *Dynamic Light Scattering*, Wiley Interscience, New York.
- Cai, J., Lu, N., and Sorensen, C. M. (1995). Analysis of fractal cluster morphological parameters: Structural coefficient and density autocorrelation function cutoffs, *J. Coll. Inter. Sci.* 171:470–473.
- Chan, P., and Dahneke, B. (1981). Free-molecule drag on straight chains of uniform spheres, *J. Appl. Phys.* 52:3106–3110.
- Forrest, S. R., and Witten, Jr., T. A. (1979). Long-range correlations in smoke-particle aggregates, *J. Phys. A: Math. Gen.*, 12:L109–L117.
- Friedlander, S. K., and Wang, C. S. (1966). The self-preserving particle size distribution for coagulation by Brownian motion, *J. Colloid Interface Sci.* 22:126–132.
- Friedlander, S. K. (1977). *Smoke, Dust, and Haze*, Wiley-Interscience, New York.
- Lai, F. S., Friedlander, S. K., Pich, J., and Hidy, G. M. (1972). The self-preserving particle size distribution for Brownian coagulation in the free molecular regime, *J. Colloid Inter. Sci.* 39:395–411.
- Lin, M. Y., Lindsay, H. M., Weitz, D. A., Ball, R. C., Klein, R., and Meakin, P. (1990). Universal reaction-limited colloid aggregation, *Phys. Rev. A* 41:2005–2020.
- Lushnikov, A. A. (1973). Evolution of coagulation system, *J. Colloid Interface Sci.* 45:549–556.
- Mandelbrot, B. B. (1982). *Fractal Geometry Of Nature*, W. H. Freeman, San Francisco, CA.
- Matsoukas, T., and Friedlander, S. K. (1991). Dynamics of aerosol agglomerate formation, *J. Colloid Inter. Sci.* 146:495–605.
- Meakin, P., Donn, B., and Mulholland, G. W. (1989). Collision between point masses and fractal aggregates, *Langmuir* 5:510–518.
- Mulholland, G. W., Sampson, R. J., Mountain, R. D., and Ernst, M. H. (1988). Cluster size distribution for free molecular agglomeration, *J. Energy Fuels* 2:481–486.
- Oh, C., and Sorensen, C. M. (1997a). Light scattering study of fractal cluster aggregation near the free molecular regime, *J. Aerosol Sci.* 28:937–957.
- Oh, C., and Sorensen, C. M. (1997b). The effect of monomer overlap on the morphology of fractal aggregates, *J. Coll. Inter. Sci.* 193:17–25.
- Okuyama, K., Kousaka, Y., Tohge, N., Yamamoto, S., Wu, J. J., Flagan, R. C., and Seinfeld, J. H. (1986). Production of ultrafine metal oxide particles by thermal decomposition of metal alkoxide vapor, *AIChE Journal* 32:2010–2022.
- Olivier, B. J., and Sorensen, C. M. (1990). Aggregation kernel homogeneity dependence on aggregate concentration in gold colloids, *Phys. Rev. A* 41:2093–2100.
- Olivier, B. J., Sorensen, C. M., and Taylor, T. W. (1992). Scaling dynamics of aerosol coagulation, *Phys. Rev. A* 45:5614–5623.
- Schaefer, D. W., and Berne, B. J. (1972). Light scattering from non-Gaussian concentration fluctuation, *Phys. Rev. Lett.* 28:475–478.
- Sorensen, C. M. (1997). *Scattering and Absorption of Light by Particles and Aggregates, Handbook of Surface and Colloid Chemistry*, Edited by K. S. Birdi. CRC Press, Boca Raton.
- Sorensen, C. M., and Roberts, G. C. (1997). The prefactor of fractal aggregates, *J. Coll. Inter. Sci.* 186:447–452.

¹In Olivier et al. (1992), we erroneously left out the Epstein regime for which $\lambda = -1/3$ and only considered the ballistic regime when $\text{Kn} \gg 1$ for which $\lambda = 1/6$.

- Sorensen, C. M., and Wang, G. M. (1999). Size distribution effect on the power law regime of the structure factor of fractal aggregates, *Phys. Rev. E* 60:7143–7148.
- Sorensen, C. M., and Wang, G. M. (1999). Note on the correction for diffusion and drag in the slip regime, *Aerosol Sci. Tech.* 33:353–356.
- Rogak, S. N., and Flagan, R. C. (1992). Coagulation of aerosol agglomerates in the transition regime, *J. Colloid Inter. Sci.* 151:203–224.
- van Dongen, P. G. J., and Ernst, M. H. (1985). Dynamic scaling in kinetics of clustering, *Phys. Rev. Lett.* 54:1396–1399.
- Viscek, T. (1992). *Fractal Growth Phenomena*, World Scientific, San Francisco, CA.
- Wagner, P. E., and Kerker, M. (1977). Brownian coagulation of aerosols in rarefied gases, *J. Chem. Phys.* 66:638–646.
- Wang, C. S., and Friedlander, S. K. (1967). The self-preserving particle size distribution for coagulation by Brownian motion II. Small particle slip correction and simultaneous shear flow, *J. Colloid Interf. Sci.* 24:170–180.
- Wang, G. M., and Sorensen, C. M. (1999). Diffusive mobility of fractal aggregates over the entire Knudsen number range, *Phys. Rev. E* 60:3036–3044.
- Weitz, D. A., Huang, J. S., Lin, M. Y., and Sung, J. (1984). Dynamics of diffusion limited kinetic aggregation, *Phys. Rev. Lett.* 53:1657–1700.
- Weitz, D. A., Huang, J. S., Lin, M. Y., and Sing, J. (1985). Limits of the fractal dimension for irreversible kinetics of aggregation of gold colloids, *Phys. Rev. Lett.* 54:1416–1419.

NOMENCLATURE

- a Monomer (or primary) particle radius.
- A Coefficient determining cross over of diffusion from Stokes–Einstein to Epstein, see Equation (8).
- A Normalization constant for the scaling function, see Equation (19).
- B_0, B_1, B_2, B_3 Coefficients involved in $C(t)$.
- c A constant of order unity.
- $C(t)$ Scattered light intensity autocorrelation function.
- D Diffusion coefficient.
- D_f The fractal dimension.
- $D(u)$ Diffusion coefficient of aggregate with u monomers.
- D_{SE} Stokes–Einstein diffusion coefficient.
- D_{Ep} Epstein diffusion coefficient.
- k Boltzmann’s constant.
- k_o A constant of order unity (≈ 1.3 for DLCA), see Equation (1).
- $K(x, y)$ Aggregation kernel.
- Kn The Knudsen number, the ratio of the medium molecule mean free path to the particle mobility radius.
- m Molecular mass.
- mfp Medium molecule mean free path.
- M_i i th moment of the aggregate size distribution, see Equation (18).
- $n(v, t)$ Number density of aggregates with v monomers at time t .
- N Number of monomers per aggregate.
- q The scattering wave vector.
- R Particle or aggregate radius used generically.
- R_g Radius of gyration of an aggregate.
- R_m Mobility radius.
- s Exponent describing functionality of the diffusion coefficient on the Knudsen number.
- s_p Mean number of monomers per aggregate.
- t_o Initial time.
- t_c Characteristic aggregation time.
- t_{exp} Experimental run time, see Figure 5.
- T Absolute temperature.
- x Exponent describing functionality of the mobility radius on number of monomers per aggregate, see Equation (11).
- z The dynamic exponent, $z = (1 - \lambda)^{-1}$.
- α Constant involved in the scaling function, see Equation (19).
- β Accommodation coefficient.
- η Medium shear viscosity.
- θ The scattering angle.
- λ The degree of homogeneity of the aggregation kernel.
- λ_o Wavelength of light.
- ρ Medium mass density.
- τ_c The correlation time.
- τ_2, τ_3 Fit variables for $C(t)$.
- $\phi(v)$ The scaling function of the size distribution, see Equation (15).